Article

Insight into the Dual Cycle Mechanism of Methanol-to-Olefins Reaction over SAPO-34 Molecular Sieve by Isotopic Tracer Studies

YU Bowen[1,2], LOU Caiyi[1,2], ZHANG Wenna[1], XU Shutao[1], HAN Jingfeng[1], YU Zhengxi[1], WEI Yingxu[1*] and LIU Zhongmin[1*]

1. National Engineering Laboratory for Methanol to Olefins, Dalian National Laboratory for Clean Energy, iChEM(Collaborative Innovation Center of Chemistry for Energy Materials), Dalian Institute of Chemical Physics, Chinese Academy of Sciences, Dalian 116023, P. R. China;

2. University of Chinese Academy of Sciences, Beijing 100039, P. R. China

Abstract Methanol-to-olefins(MTO) reaction is one of the important non-petroleum routes to produce light olefins over acidic molecular sieves. In this study, the complete reaction course of MTO on SAPO-34 molecular sieve with retained organics evolution from induction period to deactivation period was investigated systematically at different weight hourly space velocities(WHSV) of methanol. By the aid of $^{12}C/^{13}C$-methanol isotopic switch experiment, the dual cycle mechanism involving aromatics-based cycle and alkenes-based cycle was evaluated during the whole reaction process. The detailed reaction route varied with the evolution of the retained organics in the catalyst at different reaction stages. The aromatics-based cycle and alkenes-based cycle alternately dominate the reaction process. In the efficient reaction period, aromatics-based cycle is the main reaction mechanism, while in the induction and deactivation periods, the contribution of alkenes-based cycle mechanism will become more important.

Keywords SAPO-34; Methanol-to-olefin(MTO); Polymethylbenzene; Dual-cycle mechanism; Isotopic tracer

1 Introduction

Methanol-to-olefins(MTO) reaction over acidic molecular sieves as a non-petroleum route to produce the light olefins, such as ethene and propene, has attracted extensive interests from academy and industry[1—3]. SAPO-34 molecular sieve with 8-membered ring pore opening, chabazite(CHA) topology and relatively moderate acidity has been applied in the commercial MTO process[4].

The mechanism of MTO has been studied extensively over four decades[1,2,5—7]. A lot of studies have been concerned on the direct mechanism[8—17] and the indirect mechanism[18—34]. In recent studies, the first C—C bond formation was deeply understood by different groups using different characterization methods[8—13]. Fan's group[12] proposed a crucial intermediate of methoxymethyl cations($CH_3OCH_2^+$) and its subsequent transformation with dimethyl ether(DME) or methanol to $CH_3OCH_2CH_2OR$(R=H or CH_3) for the first C—C bond formation by *in situ* infrared spectroscopy. Lercher's group[13] postulated that acetate species could lead to the formation of dimethoxymethane(DMM) and the carbon-carbon bond formation was further demonstrated by Weckhuysen's group[14] using 2D ^{13}C-^{13}C solid state NMR(ssNMR) spectroscopy. Deng's group[15] proposed that surface methoxy species bonded to an extra-framework aluminum was responsible for the formation of the first C—C bond. In 2015, our group[16] investigated the behaviors for induction period of MTO reaction by kinetic method and distinguished three reaction stages of induction period, *i.e.*, the initial C—C bond formation stage, the hydrocarbon pool(HCP) species formation stage and the autocatalysis reaction stage. Furthermore, using *in situ* ^{13}C ssNMR and 2D ^{13}C-^{13}C ssNMR spectroscopy, a surface methyleneoxy analogue originated from the activation of surface-adsorbed DME with methoxy was captured. This is the first time that achieved direct spectroscopic evidence for the C1 reactants activation and the first C—C bond formation[17,18]. For the efficient reaction stage, the indirect mechanism, such as hydrocarbon pool(HCP) mechanism was proposed and supported by both experimental and theoretical evidences in this efficient stage of MTO reactions[18—33]. According to this mechanism, methanol reacted

*Corresponding authors. Email: weiyx@dicp.ac.cn; liuzm@dicp.ac.cn

Received June 29, 2020; accepted August 3, 2020.

Supported by the National Key R&D Program of China(No.2018YFB0604901), the National Natural Science Foundation of China(Nos.21991090, 21991092, 21972142, 91834302, 91745109), the Liaoning Revitalization Talents Program, China(Nos. XLYC1808014, XLYC1807227), the Youth Innovation Promotion Association of the Chinese Academy of Sciences, China(No. 2014165), the Key Research Program of Frontier Sciences of the Chinese Academy of Sciences (Nos.QYZDY-SSW-JSC024, QYZDB-SSW-SLH026), the International Partnership Program of the Chinese Academy of Sciences(No.121421KYSB20180007) and the Strategic Priority Research Program of the Chinese Academy of Sciences(No.XDA21030200).

with the HCP species, which were retained in the catalysts and the light olefins were split off from these species. Aromatics-based cycle including side-chain methylation route and paring route had been considered as a dominated route on SAPO-34 molecular sieve due to relatively larger cage and smaller opening pore, while dual cycle routes involving of aromatics-based cycle and alkenes-based cycle have been demonstrated reasonably on ZSM-5 zeolite[27—33]. For aromatics-based cycle mechanism, polymethylbenzenes, polymethylcyclopentadiene and their corresponding carbenium ions were considered to be the main active HCP species on H-SAPO-34 and H-beta catalysts[34,35]. For alkenes-based cycle, light olefins were produced through alkene methylation and cracking reaction, in which alkene species were identified as the intermediates. Dai *et al.*[36] and Wang *et al.*[37] both illustrated alkenes-based cycle may occur on SAPO-34 at the early stage of MTO reaction. Dai *et al.*[36] observed three-membered ring compounds, trimethylcyclopropane and dienes confined in H-SAPO-34 *via* UV-Vis as well as ^{1}H and ^{13}C MAS NMR spectroscopy and proposed that the olefin-based catalytic cycle is the primary reaction pathway during the early stage of the MTO reaction based on these olefins-like active species. Wang *et al.*[37] demonstrated the energy feasibility of olefins-based routes for ethene and propene formation during methanol conversion over H-SAPO-34 by comparing computed overall reaction barriers of aromatics-based side-chain dealkylation and olefins-based *β*-scission process *via* density functional theoretical calculation.

In this work, methanol reaction tests were performed at 350 °C with different weight hourly space velocities(WHSV) of methanol to obtain a whole course of the methanol conversion including induction period, efficient reaction period and deactivation period. By joint analysis of GC/MS and $^{12}C/^{13}C$ switch experiments, the retained organic species have been analyzed during methanol conversion at 350 °C with a WHSV of 6 h^{-1}. In line with the results of $^{12}C/^{13}C$-CH_3OH switch experiments, the significance of aromatics-based cycle and alkenes-based cycle of dual-cycle mechanism for olefin generation from methanol conversion were clarified during different reaction stages.

2 Experimental

2.1 Sample Preparation

H-SAPO-34 containing 6% silicon[Si/(Si+Al+P)=0.06, in mole ratio] was synthesized following the method described in the literature[38].

2.2 Methanol Conversion Tests

Catalytic tests of methanol conversion were performed in a fix-bed quartz tubular reactor under atmospheric pressure. H-SAPO-34 catalysts(10—100 mg, 40—60 meshes) were loaded in the reactor and then activated at 500 °C by He with a flow rate of 25 mL/min for 1 h. Then the temperature was reduced to 350 °C. The methanol was fed by He carrier gas through a methanol saturator at 14 °C to give a He/CH_3OH ratio of 10:1 and WHSV from 2 $g_{methanol}\cdot g^{-1}_{catalyst}\cdot h^{-1}$ to 20 $g_{methanol}\cdot g^{-1}_{catalyst}\cdot h^{-1}$. The analysis method of gas-phase products and the calculation method of methanol conversion and product selectivity had been described in our previous work[39].

请确认此处的表示单位是否有误
更改为：2 h-1

2.3 $^{12}C/^{13}C$-methanol Switch Experiments

In $^{12}C/^{13}C$-methanol switch experiments, $^{12}CH_3OH$ was fed firstly for a certain time, then $^{12}CH_3OH$ feed was ceased and methanol feed was switched to $^{13}CH_3OH$ for further 1 min. The isotopic distribution of gas-phase effluents and the organic species retained in H-SAPO-34 catalysts was analyzed and determined by online GC-MS. The organic species confined in H-SAPO-34 catalysts were analyzed by GC-MS(Agilent GC 7890A/5975C GC/MSD) after dissolving the catalysts in 20% hydrofluoric acid for 30 min and extracting hydrocarbons with dichloromethane(CH_2Cl_2), following the procedures introduced by Guisnet[40].

3 Results and Discussion

3.1 Methanol-to-Olefins Reaction over H-SAPO-34

The structural characterizations, such as XRD, SEM and NMR of H-SAPO-34 have been reported in our previous work[41]. The sample used here had a good crystallinity and a local chemical structure.

The high initial conversion of methanol over H-SAPO-34 at a temperature higher than 400 °C may cause a great difficulty in the direct observation of the complete reaction course, especially the induction period that is very difficult to be captured and studied[42]. Therefore, MTO reaction over H-SAPO-34 performed at a relatively lower temperature should be conducted for a complete prospect of MTO reaction. Considering the special deactivation mode of MTO reaction with adamantane hydrocarbons formed and confined in the catalyst as the deactivation species, the reaction was not conducted at very low temperature of 300 °C[43]. For the complete reaction course investigation, in the present work, methanol conversion was performed at 350 °C to explore the reactions during the three reaction periods. Fig.1 shows the methanol conversion with time on stream(TOS) over H-SAPO-34 at 350 °C under different WHSV of methanol and the selectivity of gas phase effluents is given in Table S1—Table S5(see the Electronic

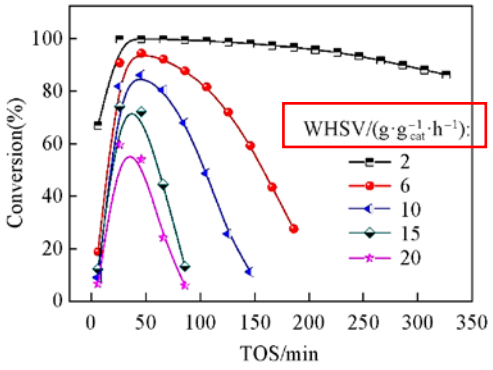

请确认WHSV的单位更改为h-1

Fig.1 Methanol conversion with time on stream over H-SAPO-34 at 350 °C under different WHSV

Supplementary Material of this paper). All reaction curves present induction periods at the beginning of the reaction, but the highest conversion is different and depends on WHSV. When the WHSV was 2 h^{-1}, the conversion of methanol at TOS of 6 min was 66.96%, and then it increased quickly with reaction time to nearly 100% at 50 min and the conversion kept >90% for nearly 300 min. When the WHSV was set at 6 h^{-1}, the initial conversion of methanol at 6 min was only 19%, then conversion was enhanced in the following reaction period to 94.52% at 46 min, exhibiting a typical feature of low conversion efficiency during the induction period and a very high efficient reaction during the efficient reaction stage. After the efficient reaction stage, conversion of methanol decreased to 27.75% at 186 min, indicating the occurrence of deactivation. The three reaction stages of induction period, efficient reaction period and deactivation period corresponded to the reaction at 0—30 min, 30—70 min and 70—190 min, respectively. Higher WHSV caused methanol penetrating through the catalyst bed and the conversion of methanol would decrease to some extent at the same reaction time. For all the reactions performed with different WHSV of methanol, light olefins, such as ethene, and propene generated as the main products, the variation of the product selectivity with time on stream was very similar even the differences in lifetime. In order to understand deeply the difference of conversion rate under different WHSV, we changed the horizontal axis from TOS to WHSV×TOS and obtained the variation of methanol conversion with the amount of methanol feeding(Fig.S1, see the Electronic Supplementary Material of this paper). For the same reactant feeding amount, the reaction performed under a larger WHSV showed the lower conversion efficiency of methanol. This implied that more methanol was required to be fed to overcome the induction period.

3.2 Retained Organic Species in H-SAPO-34

In order to explain the variation of methanol conversion over H-SAPO-34 during the whole reaction course, the formation and evolution of retained organics formed in the CHA nanocages with reaction time were studied. GC-MS analysis was applied to identifying the retained organic species during methanol conversion over H-SAPO-34 at 350 °C with a WHSV of 6 h^{-1}. Previous work[41] gave the detailed reaction performance of the sampling point during MTO reaction and deactivation.

The evolution of organic species with different reaction time is shown in Fig.2 and the assignments of them were presented in Table 1. For clarification, the retained organic species are classified into five groups: lower methylated benzenes(lower MBs, the number of substituted methyl groups was from 1 to 3), higher methylated benzenes(higher MBs, the number of substituted methyl groups was from 4 to 6), adamantane derivatives, methylnaphthalenes, and polyaromatic hydrocarbons(phenanthrene and pyrene). In the induction period of the reaction, polymethylbenzenes as the active hydrocarbon pool species were formed and increased with reaction time. They contributed to the high methanol conversion in the efficient reaction period until the methylnaphthalenes intensity increased obviously in the later stage of this period. In the deactivation period, polyaromatic hydrocarbons began to accumulate and the methanol conversion

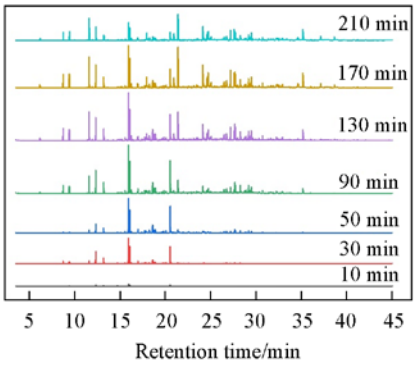

Fig.2 Evolution of retained hydrocarbon compounds confined in the H-SAPO-34 catalysts with time on stream at 350 °C under methanol WHSV of 6 h^{-1}

Table 1 Identification of retained hydrocarbon compounds confined in the H-SAPO-34 catalyst by GC-MS

Retention time/min	Compound	Structure
6.1	Toluene	
8.73, 9.4	Xylene	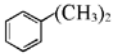
11.58, 12.3, 13.2	TriMB	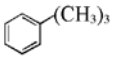
15.95, 16.07	TetraMB	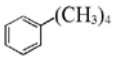
20.5	PentaMB	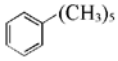
24.93	HMB	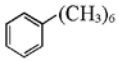
16.27, 18.02, 18.77, 18.91	TriMA	
17.4	DiMA	
17.7, 17.85, 18.6	MA	
17.92	Naphthalene	
20.95, 21.41	MN	
24.14, 24.23, 24.66, 24.73, 25.02	DiMN	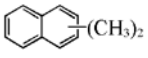
27.19, 27.58, 27.98	TriMN	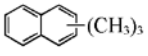
29.47	TetraMN	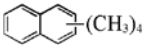
32.21	Phenanthrene	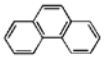
38.66	Pyrene	

decreased accordingly. Beside methylnaphthalenes, some lower benzenes, such as toluene, xylene and trimethylbenzenes, presenting very low reactivity towards methanol conversion, were also intensified during deactivation period. In order to clarify the contribution of these confined organic species for olefins production, the isotopic tracer technique was employed for investigation.

确认此处是否正确
正确

3.3 $^{12}C/^{13}C$-methanol Switch Experiments

Polymethylbenzenes were considered to be “MTO engines” and previous studies have proved their high reactivity in methanol conversion[21—29]. The results of $^{12}C/^{13}C$ methanol switch experiments also indicated the more involvement of polymethybenzenes, such as hexamethylbenzene in methanol conversion than the lower methylbenzenes, not only at the induction but also during the deactivation period[44]. For a systematic comprehension of the function of these confined organics in the reaction and deactivation, $^{12}C/^{13}C$-methanol switch experiment was performed over H-SAPO-34 in different reaction stages to measure the reactivity evolution of the retained materials, such as methylbenzenes, methylnaphthalenes and adamantane hydrocarbons.

After ^{12}C-methanol conversion over H-SAPO-34 at 350 °C for 10, 50, 130 and 210 min, the feed was switched to ^{13}C-methanol for 1 min. Fig.3 shows the ^{13}C content of products in gas-phase and the retained organics in H-SAPO-34 catalysts. The results indicated that during the induction period, such as TOS of 10 min, all the methylbenzene species, including both lower MBs and higher MBs, exhibited relatively higher ^{13}C content than other reaction stages. The gas phase products also exhibited the highest ^{13}C content in the induction period. Initial olefins generation was mainly from the reaction route of direct mechanism[17], which contributed to produce the ^{13}C-ethene directly by $^{13}CH_3OH$. Other higher olefins were formed mainly by olefin methylation-cracking route with the $^{13}CH_3OH$ as the methylation reagent. Then the polymethylbenzene species were formed from these ^{13}C-labelled olefins through polymerization, cyclization, hydride transfer reactions and accumulated in the SAPO-34 catalyst[45]. When ^{13}C-methanol was fed over H-SAPO-34 for 1 min after continuous flow ^{12}C-methanol conversion for 50 min, more ^{13}C atoms were incorporated into PentaMB and HexaMB, representing their higher reactivity than lower MBs when contacting with methanol. Meanwhile, an improved methanol conversion was found, illustrating the functions of PentaMB and HexaMB as more reactive intermediates. Even in the deactivation stage, PentaMB and HexaMB still maintained higher reactivity than other methylbenzenes, demonstrating their important roles as reactive intermediates for methanol conversion. The decline of methanol conversion during deactivation was related with the concentration reduction of PentaMB and HexaMB in the catalyst and the concentration increase of bulky polyaromatic species. In this period, bulky and inert aromatic compounds, such as methylnaphthalene, phenanthrene and pyrene were intensified and their occupation in the catalyst cages depressed the consecutive production of reactive intermediates of polymethylbenzenes.

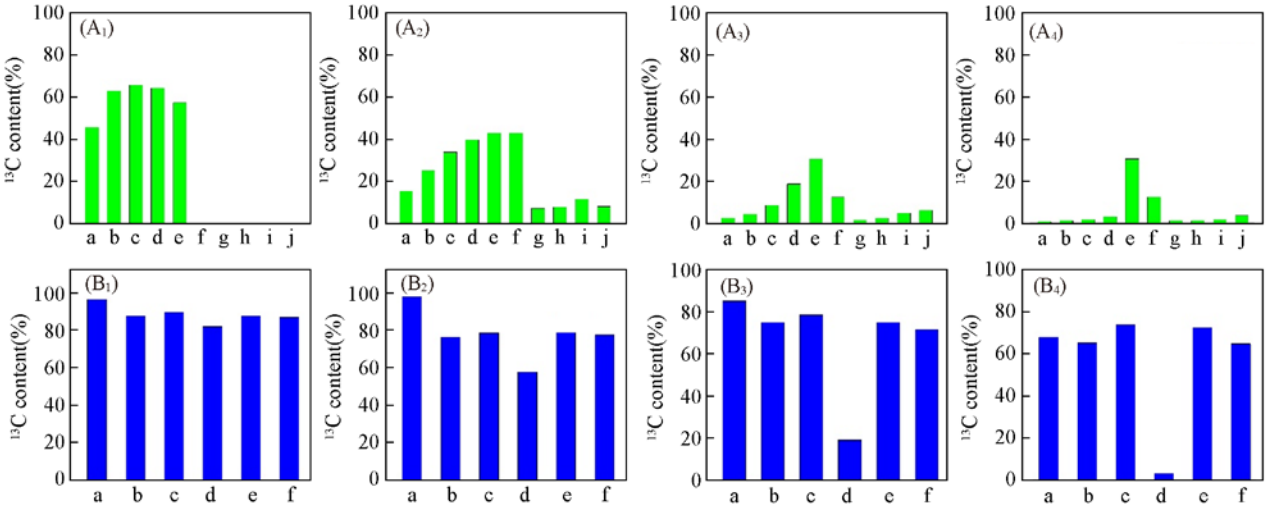

Fig.3 ^{13}C content of retained organic species(A) and gas-phase products(B) over H-SAPO-34 after $^{12}C/^{13}C$-methanol switch experiments with ^{12}C-methanol feeding followed by ^{13}C-methanol feeding for 1 min

Conducted at time on stream of 10(A_1, B_1), 50(A_2, B_2), 130(A_3, B_3) and 210 min(A_4, B_4), respectively. The reaction temperature is 350 °C and the WHSV is 6 h^{-1}. (A_1—A_4) a. Toluene; b. xylene; c. TriMB; d. TetraMB; e. PentaMB; f. HexaMB; g. Naphthalene; h. MN; i. DiMN; j. DiMA; (B_1—B_4) a. CH_4; b. C_2H_4; c. C_3H_6; d. C_3H_8; e. C_4H_8; f. C_5H_{10}.

Adamantane hydrocarbons, such as methyladamantane and dimethyladamantane, also appeared as retained compounds with a very low ^{13}C content in Fig.3. The low ^{13}C content of them after isotopic switch experiment illustrated their inert property. Our previous studies[43] found that adamantine and its derivatives formed in the cages of H-SAPO-34 at low temperature of 300 °C and accounted for the catalyst deactivation in low temperature methanol reaction. In Fig.4, the mass spectra of three retained species, tetramethylbenzene, dimethyladamantane, dimethylnaphthalene before and after $^{12}C/^{13}C$ switching experiments at 350 °C for 50 min are displayed. The scramble of ^{13}C atoms indicated that much more ^{13}C atoms

from ^{13}C-methanol were incorporated in pentamethylbenzene than dimethyladamantane and dimethylnaphthalene when contacting with the feed of ^{13}C-methanol. Therefore, polymethylbenzenes were proved to be the reactive HCP species in the efficient reaction period. The formation of methylnaphthalenes in H-SAPO-34 with very low reactivity caused the catalyst deactivation under the reaction condition. In our recently work[41], the procedure of methylnaphthalene formation was suggested by combining the experimental observation and theoretical calculation.

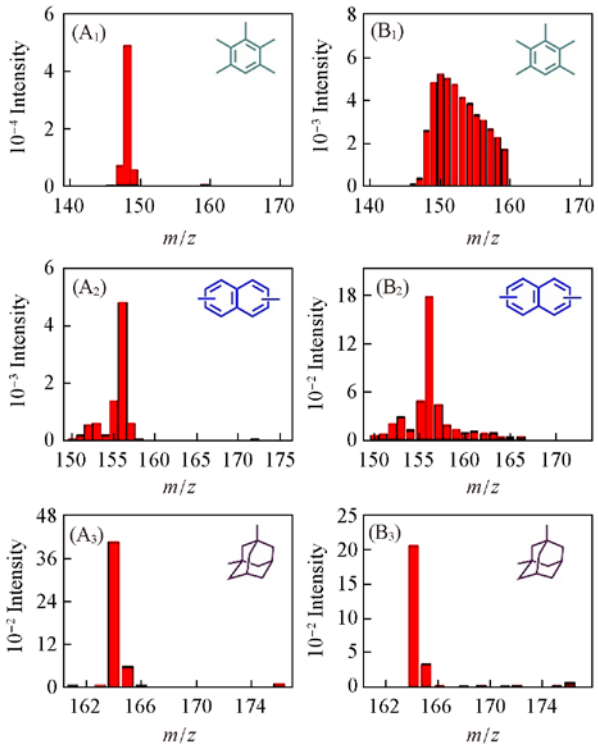

Fig.4 ^{13}C mass spectra of the confined organic species in H-SAPO-34 before(A) and after(B) ^{12}C/^{13}C methanol switch experiment at 350 °C for 50 min

(A_1, B_1) Tetramethylbenzene; (A_2, B_2) dimethyladamantane; (A_3, B_3) dimethylnaphthalene.

3.4 Dual Cycle Mechanism of MTO Reaction on H-SAPO-34

The study presented in Section **3.2** revealed that the evolution of the confined organics, including the reactive HCP species and deactivated species, were responsible for the efficient methanol conversion and deactivation, respectively. At the same time, the amount and reactivity of these confined organics also varied the reaction route. With the generation and accumulation of active HCP species during the induction period, the highest ^{13}C contents of gas phase products at TOS of 10 min presented in Fig.3 indicated the important roles of direct mechanism for initial ethene formation and the alkenes-based cycle mechanism for other olefins formation. Furthermore, the relatively closer ^{13}C content of retained HCP species and olefin products also confirmed the important role of aromatics-based cycle mechanism during the efficient reaction period. Prolonging the reaction time to 130 and 210 min, with the formation of bulky and inert coke species, ^{13}C content presented relatively larger difference between effluent gas-phase products, such as ethene and propene, and organic species confined in the catalyst. The enlarged gap of ^{13}C content between effluent olefins and retained polymethylbenzenes implied that aromatics-based cycle mechanism became less significant in deactivation period. Alternatively, olefin methylation-cracking route became relatively more dominant during this period. As indicated in Fig.2, with the formation of polyaromatics, such as methynaphthalenes, phenatharene and pyrene, the mass transfer in H-SAPO-34 catalyst was largely reduced and the reactant of methanol could not efficiently contact with the retained organics confined in the cage of H-SAPO-34. During the deactivation period, polymethylbenzene, the important reactive HCP species retained in the catalyst, from which olefin products can be eliminated, can not be consecutively generated by the methylation of methylbenzene with methanol. This also led to the decrease in the concentration of HCP species and the reaction *via* the aromatics-based cycle mechanism was depressed in this way. Comparatively, methanol conversion *via* the alkenes-based cycle reaction route with olefin methylation and cracking was not very space-required. Thus, with the occurrence of coke formation, the reaction route *via* the alkenes-based cycle became more predominant route than the aromatics-based cycle. Both of the methanol conversion and the detailed reaction routes for olefins generation were closely related with the formation and function of confined organics in the catalyst, including the important reactive intermediates for olefins generation and coke species that caused the deactivation.

4 Conclusions

A careful study of reaction, coke deposition and reaction mechanism of methanol conversion over H-SAPO-34 catalyst gave a more real and complete prospect of the reaction and deactivation. Induction period was observed at 350 °C during the reaction. The variation of methanol conversion with time on stream was correlated to the formation and evolution of confined organics in the catalyst. By the aid of GC-MS and ^{12}C/^{13}C-methanol switch techniques, the confined organics in the catalyst were analyzed and the evolution of retained species involvement in the reaction were clarified. The reaction route for olefins generation varied with the evolution of the confined organics in the catalyst during different reaction periods. In the induction period, the direct mechanism and alkenes-based cycle mechanism are mainly responsible for initial ethene and other olefins formation, respectively. Polymethylbenzenes, the most reactive intermediates formed in the induction period and accumulated with reaction time, are responsible for the highly efficient methanol conversion through aromatics-based cycle in the following reaction stage, the efficient reaction period. After that, polyaromatics species including methylnaphthalenes, phenatharene and pyrene accumulated in the deactivation period, which depressed the continuous formation of polymethylbenzenes and resulted in the deactivation. Aromatics-based cycle mechanism dominated in the efficient reaction period, while alkenes-based cycle took into effect in the induction

period and deactivation period. These findings and understandings could help to optimize the catalyst and process for the development of new generation MTO technology.

Electronic Supplementary Material

Supplementary material is available in the online version of this article at http://dx.doi.org/10.1007/s40242-020-0216-x.

References

[1] Stöcker M., *Microporous Mesoporous Mater*., **1999**, *29*, 3

[2] Olsbye U., Svelle S., Bjørgen M., Beato P., Janssens T. V. W., Joensen F., Bordiga S., Lillerud K. P., *Angew. Chem. Int. Ed*., **2012**, *51*, 5810

[3] Tian P., Wei Y. X., Ye M., Liu Z. M., *ACS Catal*., **2015**, *5*, 1922

[4] Yang M., Fan D., Wei Y. X., Tian P., Liu Z. M., *Adv. Mater*., **2019**, *31*, 1902181

[5] Haw J. F., Song W. G., Marcus D. M., Nicholas J. B., *Acc. Chem. Res*., **2003**, *36*, 317

[6] Xu S. T., Zhi Y. C., Han J. F., Zhang W. N., Wu X. Q., Sun T. T., Wei Y. X., Liu Z. M., *Adv. Catal*., **2017**, *61*, 37

[7] Yarulina I., Chowdhury A. D., Meirer F., Weckhuysen B. M., Gascon J., *Nat. Catal*., **2018**, *1*, 398

[8] Chang C. D., Silestri A. J., *J. Catal*., **1977**, *47*, 249

[9] Clarke J. K. A., Darcy R., Hegarty B. F., O'Donoghue E., Amir-Ebrahimi V., Rooney J. J., *J. Chem. Soc., Chem. Commun*., **1986**, *5*, 425

[10] Marcus D. M., McLachlan K. A., Wildman M. A., Ehresmann J. O., Kletnieks P. W., Haw J. F., *Angew. Chem. Int. Ed*., **2006**, *45*, 3133

[11] Lesthaeghe D., van Speybroeck V., Marin G. B., Waroquier M., *Angew. Chem. Int. Ed*., **2006**, *45*, 1714

[12] Li J. F., Wei Z. H., Chen Y. Y., Jing B. Q., He Y., Dong M., Jiao H. J., Li X. K., Qin Z. F., Wang J. G., Fan W. B., *J. Catal*., **2014**, *317*, 277

[13] Liu Y., Muller S., Berger D., Jelic J., Reuter K., Tonigold M., Sanchez-Sanchez M., Lercher J. A., *Angew. Chem. Int. Ed*., **2016**, *55*, 5723

[14] Chowdhury A. D., Houben K., Whiting G. T., Mokhtar M., Asiri A. M., Al-Thabaiti S. A., Basahel S. N., Baldus M., Weckhuysen B. M., *Angew. Chem. Int. Ed*., **2016**, *55*, 15840

[15] Wang C., Chu Y. Y., Xu J., Wang Q., Qi G. D., Gao P., Zhou X., Deng F., *Angew. Chem. Int. Ed*., **2018**, *57*, 10197

[16] Qi L., Wei Y. X., Xu L., Liu Z. M., *ACS Catal*., **2015**, *5*, 3973

[17] Wu X. Q., Xu S. T., Zhang W. N., Huang J. D., Li J. Z., Yu B. W., Wei Y. X., Liu Z. M., *Angew. Chem. Int. Ed*., **2017**, *56*, 9039

[18] Wu X. Q., Xu S. T., Wei Y. X., Zhang W. N., Huang J. D., Xu S. L., He Y. L., Lin S. F., Sun T. T., Liu Z. M., *ACS Catal*., **2018**, *8*, 7356

[19] Chen N. Y., Reagan W. J., *J. Catal*., **1979**, *59*, 123

[20] Dessau R. M., Lapierre R. B., *J. Catal*., **1982**, *78*, 136

[21] Dahl I. M., Kolboe S., *J. Catal*., **1994**, *149*, 458

[22] Dahl I. M., Kolboe S., *J. Catal*., **1996**, *161*, 304

[23] Xu T., Barich D. H., Goguen P. W., Song W. G., Wang Z. K., Nicholas J. B., Haw J. F., *J. Am. Chem. Soc*., **1998**, *120*, 4025

[24] Lesthaeghe D., Horre A., Waroquier M., Marin G. B., Van Speybroeck V., *Chem. Eur. J*., **2009**, *15*, 10803

[25] Wang C., Yi X. F., Xu J., Qi G. D., Gao P., Wang W. Y., Chu Y. Y., Wang Q., Feng N. D., Liu X. L., Zheng A. M., Deng F., *Chem. Eur. J*., **2015**, *21*, 12061

[26] Xu S. T., Zheng A. M., Wei Y. X., Chen J.R., Li J. Z., Chu Y. Y., Zhang M. Z., Wang Q. Y., Zhou Y., Wang J. B., Deng F., Liu Z. M., *Angew. Chem. Int. Ed*., **2013**, *52*, 11564

[27] Li J. Z., Wei Y. X., Chen J. R., Tian P., Su X., Xu S. T., Qi Y., Wang Q. Y., Zhou Y., He Y. L., Liu Z. M., *J. Am. Chem. Soc*., **2012**, *134*, 836

[28] Lesthaeghe D., van der Mynsbrugge J., Vandichel M., Waroquier M., van Speybroeck V., *ChemCatChem*, **2011**, *3*, 208

[29] Arstad B., Nicholas J. B., Haw J. F., *J. Am. Chem. Soc*., **2004**, *126*, 2991

[30] Bjorgen M., Svelle S., Joensen F., Nerlov J., Kolboe S., Bonino F., Palumbo L., Bordiga S., Olsbye U., *J. Catal*., **2007**, *249*, 195

[31] Zhang W. N., Zhi Y. C., Huang J. D., Wu X. Q., Zeng S., Xu S. T., Zheng A. M., Wei Y. X., Liu Z. M., *ACS Catal*., **2019**, *9*, 7373

[32] Zhong J. W., Han J. F., Wei Y. X., Xu S. T., Sun T. T., Zeng S., Guo X. W., Song C. S., Liu Z. M., *Chin. J. Catal*., **2019**, *40*, 477

[33] Zhong J. W., Han J. F., Wei Y. X., Xu S. T., Sun T. T., Guo X. W., Song C. S., Liu Z. M., *Chin. J. Catal*., **2018**, *39*, 1821

[34] Song W. G., Haw J. F., Nicholas J. B., Heneghan C. S., *J. Am. Chem. Soc*., **2000**, *122*, 10726

[35] Song W. G., Nicholas J. B., Sassi A., Haw J. F., *Catal. Lett*., **2002**, *81*, 49

[36] Dai W. L., Wang C. M., Dyballa M., Wu G. J., Guan N. J., Li L. D., Xie Z. K., Hunger M., *ACS Catal*., **2015**, *5*, 317

[37] Wang C. M., Wang Y. D., Xie Z. K., *Catal. Sci. Technol.*, **2014**, *4*, 2631

[38] Liu G. Y., Tian P., Li J. Z., Zhang D. Z., Zhou F., Liu Z. M., *Microporous Mesoporous Mater*., **2008**, *111*, 143

[39] Wang J. B., Wei Y. X., Li J. Z., Xu S. T., Zhang W. N., He Y. L., Chen J. R., Zhang M. Z., Zheng A. M., Deng F., Guo X. W., Liu Z. M., *Catal. Sci. Technol*., **2016**, *6*, 89

[40] Guisnet M., *J. Mol. Catal. A*: *Chem*., **2002**, *182*, 367

[41] Yu B. W., Zhang W. N., Wei Y. X., Wu X. Q., Sun T. T., Fan B. H., Xu S. T., Liu Z. M., *Chem. Commun*., **2020**, *46*, 36

[42] Gao S. S., Xu S. T., Wei Y. X., Qiao Q. L., Xu Z. C., Wu X. Q., Zhang M. Z., He Y. L., Xu S. L., Liu Z. M., *J. Catal*., **2018**, *367*, 306

[43] Wei Y. X., Li J. Z., Yuan C. Y., Xu S. T., Zhou Y., Chen J. R., Wang Q. Y., Zhang Q., Liu Z. M., *Chem. Commun*., **2012**, *48*, 3082

[44] Hereijgers B. P. C., Bleken F., Nilsen M.H., Svelle S., Lillerud K. P., Bjorgen M., Weckhuysen B. M., Olsbye U., *J. Catal*., **2009**, *264*, 77

[45] Zhang W. N., Zhang M. Z., Xu S. T., Gao S. S., Wei Y. X., Liu Z. M., *ACS Catal*., **2020**, *10*, 4510